Available online at www.sciencedirect.com
SCIENCE DIRECT
Journal of Solid State Chemistry 179 (2006) 1659–1667
JOURNAL OF SOLID STATE CHEMISTRY
www.elsevier.com/locate/jssc

$Fe_2(AsO_4)F$: A new three-dimensional condensed fluoro-arsenate iron(II) compound with antiferromagnetic interactions

Teresa Berrocal[a], José L. Mesa[b,*], José L. Pizarro[a], Miren K. Urtiaga[a], María I. Arriortua[a], Teófilo Rojo[b,*]

[a]*Departamento de Mineralogía y Petrología, Facultad de Ciencia y Tecnología, Universidad del País Vasco, Apdo. 644, E-48080 Bilbao, Spain*
[b]*Departamento de Química Inorgánica, Facultad de Ciencia y Tecnología, Universidad del País Vasco, Apdo. 644, E-48080 Bilbao, Spain*

Received 25 November 2005; received in revised form 18 February 2006; accepted 23 February 2006
Available online 2 March 2006

Abstract

$Fe_2(AsO_4)F$ has been synthesized under mild hydrothermal conditions in the form of single crystals. The compound crystallizes in $C2/c$ monoclinic space group with the unit cell parameters $a = 13.214(1)$, $b = 6.623(1)$, $c = 10.045(1)$ Å and $\beta = 116.90(2)^\circ$ with $Z = 8$. The crystal structure consists of a three-dimensional framework constructed by two kinds of chains, A and B, with 50% of population. In the chains, the environments for the iron(II) cations show penta- and hexa-coordination. The chains establish an angle of approximately 120° between them. The disordered fluoride anions in these chains given rise to $[Fe(1)O_4F(1)_{0.5}(F(2)_{0.5})_2]$ and $[Fe(2)O_4(F(1)_{0.5})_2F(2)_{0.5}]$ edge-shared polyhedra in which the fluoride anions have occupancy factors of 50% over two distinct crystallographic sites. The IR spectrum shows the characteristic bands of the $(AsO_4)^{3-}$ groups. From the diffuse reflectance spectrum a D_q parameter of 650 cm^{-1} has been calculated for the Fe(II) d^6 high spin cation. The Mössbauer spectrum in the paramagnetic state shows a doublet that has been fitted, according to the existence of two crystallographically independent iron environments, with two Lorentzian doublets. Magnetic measurements performed between room temperature and 5 K exhibit a maximum at 22.6 K, characteristic of antiferromagnetic interactions with a estimated "J"-exchange parameter of −1.2 K.

Keywords: Hydrothermal synthesis; Crystal structure; IR; UV–visible; Mössbauer; Magnetism

1. Introduction

Materials science has been growing very fast in recent decades, giving rise to an incredible number of new phases with a non-less-amazing chemical diversity. The design of condensed phases with original physical properties, by making use of the great number of cations and arrangements that they can exhibit, is an important area in this field [1].

Since Haushalter et al. [2] synthesized the first organically templated arsenates with an open framework, $(C_4H_{12}N_2)[(V^{IV}O)_2(HAsO_4)_2(H_2AsO_4)_2]$ and $(C_2H_{10}N_2)[V^{III}(HAsO_4)_2(H_2AsO_4)]\cdot H_2O$, using the vanadyl, $(VO)^{2+}$, and V(III) cations, the number of this kind of materials has increased dramatically. The majority of the templated arsenates with an open-framework known are with the Fe(III) cation and a variety of organic diamines, such as ethylenediamine [3], 1,3-diaminobutane [4], 1,4-diazobicyclooctane [5] and piperazine [6]. However, the hydrothermally synthesized condensed arsenate materials are scarce in comparison with those obtained by the ceramic method [7].

The high versatility of the mild hydro- or solvo-thermal techniques, applied with organic diamines as regulating agents of the pH, together with the *hydrogen fluoride method* [8], that uses hydrofluoric acid as a mineralizer and as connector between the metal atoms, leads to many novel structural types the synthesis of which is not possible by other synthetic procedures.

In this work, the first iron(II) fluoroarsenate synthesized via mild hydrothermal conditions is reported. The crystal structure has been resolved from single-crystal X-ray

*Corresponding authors. Fax: +34 946013500.
E-mail addresses: qipmeruj@lg.ehu.es (J.L. Mesa), qiproapt@lg.ehu.es (T. Rojo).

0022-4596/$ - see front matter © 2006 Elsevier Inc. All rights reserved.
doi:10.1016/j.jssc.2006.02.029

diffraction data. Furthermore, the thermal behavior is analyzed, together with its UV–visible and Mössbauer spectroscopic characteristics. This phase exhibits antiferromagnetic behavior with an estimated J-exchange parameter of –1.2 K.

2. Experimental

2.1. Synthesis and characterization

$Fe_2(AsO_4)F$ was synthesized using mild hydrothermal conditions under autogeneous pressure. $Fe_2(SO_4)_3 \cdot 7H_2O$ (0.1505 g, 1.481 mmol) and $As_2O_5 \cdot 3H_2O$ (0.4205 g, 1.481 mmol) were solved in 10 ml of water and HF (1 mL, 57.5 mmol) and homopyperazine was added in order to fix the pH at 6. The reaction mixture was stirred to assure homogeneity, sealed in a PTFE-lined stainless-steel pressure vessel (fill factor 75%) and then heated at 170 °C for 5 days, followed by slow cooling to room temperature. The pH did not show any appreciable change during the hydrothermal reaction. $Fe_2(AsO_4)F$ was obtained in the form of single crystals of light brown color, the yield being 80%. The reduction from Fe(III) to Fe(II) is probably caused by the presence of the homopyperazine and the water solvent in energetic hydrothermal conditions.

The percentage of elements in the product was determined by inductively coupled plasma atomic emission spectroscopy (ICP-AES). With fluorine content requiring the use of a selective electrode. Observed: Fe, 41.0; As, 27.3; F, 6.6. $Fe_2(AsO_4)F$ requires: Fe, 41.4; As, 27.9; F, 7.0. The density, measured on a compressed pellet (2 kbar, 30 min) using a Mettler Toledo AG 204 balance, was 4.50(1) g cm^{-3}.

Thermogravimetric analysis was carried out under synthetic air in a DSC 2960 simultaneous DSC-TGA instrument. A crucible containing ca. 20 mg of sample was heated at 5 °C min^{-1} in the temperature range 30–800 °C. The thermogravimetric curve shows an exothermic mass loss of 4% at approximately 500 °C, which can be attributed to the partial elimination of the fluoride anion (calc. 7%). Above this temperature the elimination of the fluoride anions, in the form of F_2(g), is completed and, at approximately 700 °C an increase of the mass takes place due to the oxidation process Fe(II) to Fe(III) and subsequent formation of the inorganic residues formed by the monoclinic $FeAsO_4$ [$P2_1/n$, $a = 5.012$, $b = 8.081$, $c = 7.68$ Å, $\beta = 104.46°$] [9a], the trigonal $FeAsO_4$ [$P3_121$, $a = 5.027$, $c = 11.234$ Å) [9b], that is isomorphous with the trigonal $FePO_4$ [9c], and finally a triclinic oxoarsenate of iron(III), $Fe_4O_3(AsO_4)_2$ [P-1, $a = 6.461$, $b = 6.594$, $c = 5.035$ Å, $\alpha = 106.35$, $\beta = 98.46$, $\gamma = 108.71°$] [9d].

The thermal behavior was studied by time-resolved X-ray thermodiffractometry in air using a Philips X'PERT automatic diffractometer (Cu$K\alpha$ radiation) equipped with a variable-temperature stage (Paar Physica TCU 2000) with a Pt sample holder. The powder patterns were recorded in 2θ steps of 0.03° in the range $10 \leqslant 2\theta \leqslant 38.5°$ counting for 2 s per step and increasing the temperature at 15 °C min^{-1} from room temperature to 810 °C. The compound is stable up to 375 °C up to which temperature the intensity of the monitored (202) maximum at $2\theta = 27.7°$ remains practically unchanged (Fig. 1). In the 375–540 °C range a decrease of the intensity of the diffraction maxima is observed, indicating a loss of crystallinity. Above 540 °C the diffraction maxima of the monoclinic $FeAsO_4$, the trigonal $FeAsO_4$ and the triclinic oxoarsenate of iron(III), $Fe_4O_3(AsO_4)_2$ [9], appear. These

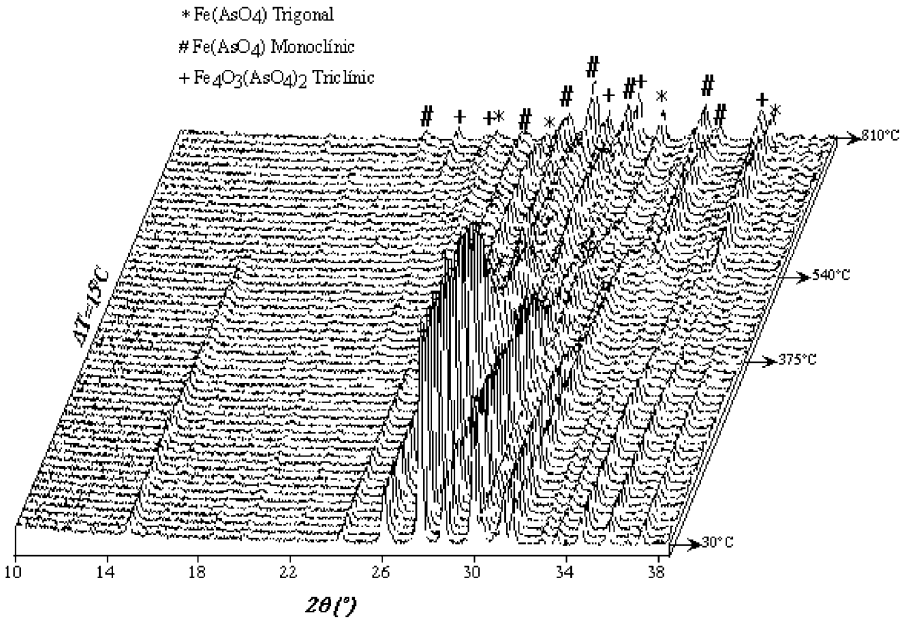

Fig. 1. Thermodiffractograms of $Fe_2(AsO_4)F$.

inorganic residues are the same as those observed in the thermogravimetric analysis.

2.2. Single-crystal X-ray diffraction

A prismatic single-crystal of the $Fe_2(AsO_4)F$ with dimensions $0.1 \times 0.05 \times 0.05$ mm was carefully selected under a polarizing microscope and mounted on a glass fiber. Single-crystal X-ray diffraction data were collected at room temperature on an Oxford Diffraction XCALIBUR2 automated diffractometer (Mo$K\alpha$ radiation) equipped with a CCD detector. In all 3096 reflections collected, 896 were independent (Rint. = 0.082) and observed applying the criterion $I \geqslant 2\sigma(I)$. The Lorentz polarization and absorption corrections were made with the diffractometer software [10], taking into account the shape and size of the single crystal. The structure was solved by direct methods with the SIR92 program [11] in the $C2/c$ space group.

Table 1
Crystallographic data and structure refinement parameters for $Fe_2(AsO_4)F$

Formula	$Fe_2(AsO_4)F$
Molecular weight ($g\,mol^{-1}$)	269.55
Crystal system	Monoclinic
Space group (No. 15)	$C2/c$
a (Å)	13.214(1)
b (Å)	6.623(1)
c (Å)	10.045(1)
β (°)	116.90(2)
V (Å^3)	784.05(1)
Z	8
ρ_{obs}, ρ_{calc}, ($g\,cm^{-3}$)	4.50(1), 4.56
$F(000)$	1008
Temperature (K)	293
Diffractometer	Oxford Diffraction Xcalibur2
μ (mm^{-1})	15.694
Radiation, λ(Mo$K\alpha$) (Å)	0.71073
Limiting indices h, k, l	± 17, $-5 \leqslant k \leqslant 8$, ± 13
R (int)	0.0824
$R[I > 2\sigma(I)]$	$R_1 = 0.0352$, $wR_2 = 0.0545$
R [all data]	$R_1 = 0.0593$, $wR_2 = 0.0597$
G. O. F	0.922

$R_1 = [(|F_o|-|F_c|)]/|F_o|$; $wR_2 = [[w(|F_o|^2-|F_c|^2)^2]/[w(|F_o|^2)^2]]^{1/2}$; $w = 1/[\sigma^2|F_o|^2 + (xp)^2 + yp]$; where $p = [|F_o|^2 + 2|F_c|^2]/3$; $x = 0.0447$, $y = 0.0$.

Table 2
Atomic coordinates, equivalent thermal parameters (U_{eq}) and occupancy factors for $Fe_2(AsO_4)F$

Atoms	x	y	z	$U_{eq} \times 10^3$	Occupancy
Fe(1)	0.4413(1)	−0.2255(2)	0.4863(2)	17(1)	1
Fe(2)	0.3433(1)	0.6079(1)	0.1308(1)	16(1)	1
As	0.3261(1)	0.1013(1)	0.1936(1)	10(1)	1
O(1)	0.3712(4)	0.2974(5)	0.1268(4)	16(1)	1
O(2)	0.2049(4)	0.1583(6)	0.2007(5)	18(1)	1
O(3)	0.3051(4)	−0.0875(5)	0.0711(4)	15(1)	1
O(4)	0.4274(4)	0.0421(6)	0.3650(4)	16(1)	1
F(1)	0.5057(6)	−0.3429(10)	0.3350(9)	23(3)	0.498(9)
F(2)	0.5316(7)	−0.4295(10)	0.4589(10)	24(3)	0.502(9)

$U_{eq} = 1/3[U_{11}(aa^*)^2 + U_{22}(bb^*)^2 + U_{33}(cc^*)^2 + 2U_{13}aca^*c^*\cos\beta]$.

Table 3
Selected bond distances (Å) and angles (°) for $Fe_2(AsO_4)F$

[Fe(1)O_4F_3] octahedron

Fe(1)	F(2)	O(1)^{i}	O(4)^{ii}	O(4)	O(2)^{iii}	F(1)	F(2)^{iv}
F(2)^{iv}	45.7(4)	71.5(2)	114.3(2)	156.9(2)	80.7(2)	75.6(3)	2.337(7)
F(1)	35.2(3)	145.9(2)	104.1(2)	81.8(2)	75.2(2)	2.192(7)	
O(2)^{iii}	89.7(3)	90.7(2)	164.6(1)	89.2(1)	2.137(4)		
O(4)	114.1(3)	129.6(1)	75.5(1)	2.113(4)			
O(4)^{ii}	98.3(3)	97.4(1)	2.093(4)				
O(1)^{i}	116.6(2)	2.064(5)					
F(2)	1.901(7)						

[Fe(2)O_4F_3] octahedron

Fe(2)	F(1)^{v}	O(3)^{vii}	O(1)	O(2)^{vi}	O(3)^{viii}	F(2)^{v}	F(1)^{viii}
F(1)^{viii}	46.3(4)	174.0(2)	93.2(2)	75.5(2)	97.5(2)	78.8(3)	2.222(8)
F(2)^{v}	34.7(3)	98.2(3)	73.3(2)	154.3(3)	96.7(2)	2.227(7)	
O(3)^{viii}	89.1(2)	77.6(1)	163.7(1)	87.5(1)	2.100(4)		
O(2)^{vi}	120.6(3)	107.4(1)	107.0(1)	2.087(5)			
O(1)	89.5(2)	90.8(1)	2.093(4)				
O(3)^{vii}	129.3(3)	2.092(4)					
F(1)^{v}	1.894(8)						

[AsO_4] tetrahedron

As	O(1)	O(2)	O(3)	O(4)
O(4)	109.1(3)	110.0(2)	111.5(1)	1.681(4)
O(3)	104.6(2)	110.7(2)	1.687(4)	
O(2)	111.0(2)	1.679(4)		
O(1)	1.689(4)			

Symmetry codes: i = $x, -y, z+1/2$; ii = $-x+1, -y, -z+1$; iii = $-x+1/2, y-1/2, -z+1/2$; iv = $-x+1, -y-1, -z+1$; v = $-x+1, y+1, -z+1/2$; vi = $-x+1/2, y+1/2, -z+1/2$; vii = $-x+1/2, -y+1/2, -z$; viii = $x, y+1, z$; ix = $x, -y, z-1/2$; x = $x, y-1, z$.

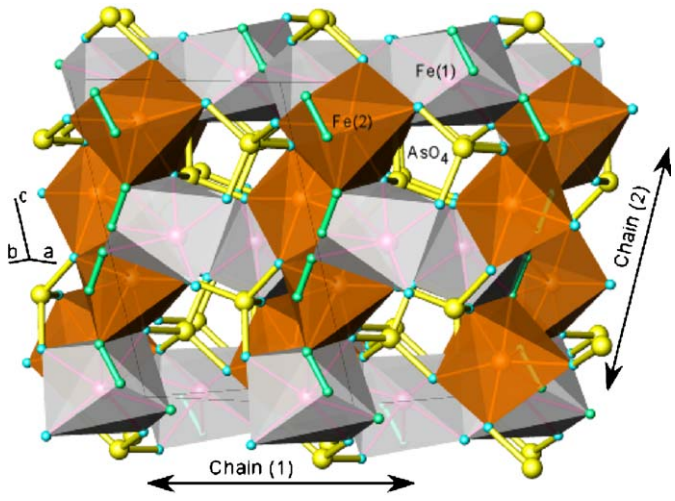

Fig. 2. Polyhedral representation of the average three-dimensional crystal structure for $Fe_2(AsO_4)F$.

Initially the positions of the iron(II) and arsenic(V) ions and three oxygen atoms were located. SHELXL97 [12] was used to refine the structure by the least-squares method based on F^2. The refinement procedure allowed to identify the rest of the oxygen and fluorine atoms. The F-atoms are disordered in two general crystallographic positions, F(1) and F(2), with occupancy factors of 50% for each site. Scattering factors were taken from Ref. [13]. Details of crystal data, intensity collection and some features of the structure refinement are given in Table 1. Anisotropic thermal parameters were used to refine all the atoms. Final *R*-factors were $R1 = 0.0593$ (all data) [w$R_2 = 0.0597$]. Maximum and minimum peaks in the final difference synthesis were 0.894, $-0.976\,e\text{Å}^{-3}$. All structure drawings were made using the ATOMS program [14]. Fractional atomic coordinates and equivalent isotropic thermal parameters are shown in Table 2. Selected bond distances and angles are given in Table 3. The CIF file has been deposited at the Cambridge Structural Data Base (CSD No. 415594).

2.3. Physicochemical characterization techniques

The IR spectrum (KBr pellets) was obtained with a Nicolet FT-IR 740 spectrophotometer in the 400–4000 cm^{-1} range. Diffuse reflectance spectrum was registered at room temperature on a Cary 2415 spectrophotometer in the 210–2000 nm range. Mössbauer

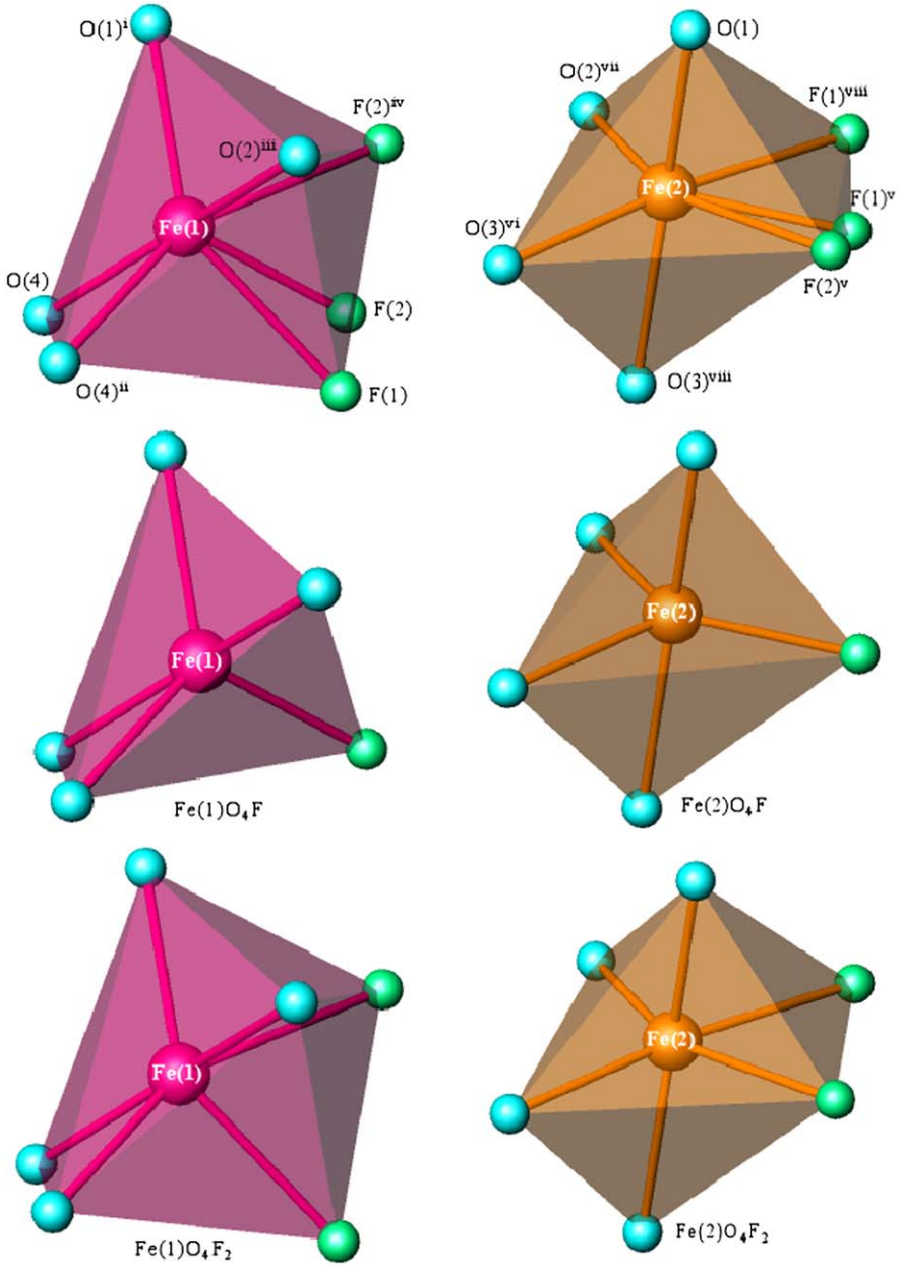

Fig. 3. Representation of the polyhedra showing the five- and hexa-coordination of the iron(II) cations.

measurements were recorded at room temperature in the transmission geometry using a conventional constant-acceleration spectrometer with a ^{57}CoRh source. Magnetic measurements on powdered sample were performed in the temperature range 5–300 K, using a Quantum Desingn MPMS-7 SQUID magnetometer. The applied magnetic field was 0.1 T, a value in the range of linear dependence of magnetization vs. magnetic field, even at 5 K.

2.4. Description of the crystal structure

The crystal structure of $Fe_2(AsO_4)F$ consists of a three-dimensional framework constructed from iron(II)–oxygen–fluorine polyhedra and arsenate groups (Fig. 2).

The iron(II) polyhedra can be described as $[Fe(1)O_4F(1)_{0.5}(F(2)_{0.5})_2]$ and $[Fe(2)O_4(F(1)_{0.5})_2F(2)_{0.5}]$. The subscripts 0.5 on the fluoride anions are included in order to note that these ions have 50% of occupancy in each position. The disorder of these anions in the metallic polyhedra gives rise to $[Fe(1)O_4F_{1.5}]$ and $[Fe(2)O_4F_{1.5}]$ units, in which the F(1)–F(1)^{x} [x = $-x+1$, $y, -z+1$] and F(2)–F(2)^{iv} [iv = $-x+1, -y-1, -z+1$] distances have a small value of 1.65(2) and 1.70(1)Å, respectively (Fig. 3). Due to this crystallochemical feature, the observed iron polyhedra can be described as an average of FeO_4F and FeO_4F_2, with coordination numbers of 5 and 6, respectively.

For the $[Fe(1)O_4F_{1.5}]$ and $[Fe(2)O_4F_{1.5}]$ average polyhedra the Fe(1),Fe(2)–O bond distances are in the 2.064(5)–2.137(4) and 2.087(5)–2.100(4) Å ranges, respectively. The Fe(1), Fe(2)–F bond lengths range from 1.901(7) to 2.337(7) and from 1.894(1) to 2.227(7) Å, respectively. The *cis*-(F,O)–Fe(1)–(O,F) and *cis*-(F,O)–Fe(2)–(O,F) angles are in the range of 45.7(4)–129.6(1)° and 46.3(4)–129.5(3)°, respectively. Finally, the

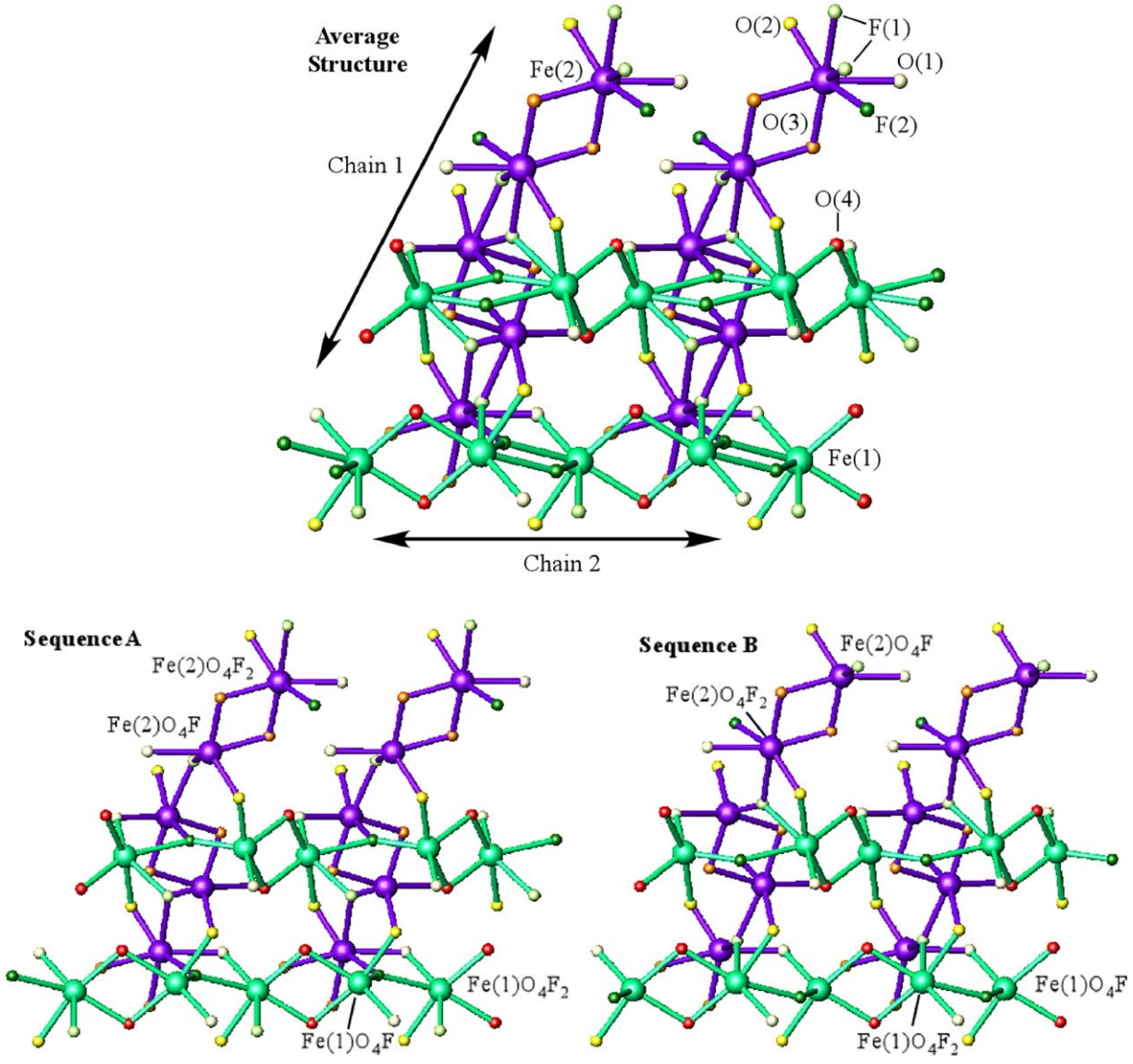

Fig. 4. View of the sequences A (hexa- and five-coordination) and B (five and hexa-coordinations) for the chains in the three-dimensional crystal structure of $Fe_2(AsO_4)F$. The average of the sequences A and B gives the three-dimensional disordered crystal structure of the $Fe_2(AsO_4)F$ phase.

trans-(F,O)–Fe–(O,F) bond angles range from 145.9(2) to 164.6(1)° for Fe(1) and from 154.3(3) to 174.0(2)° for Fe(2).

These polyhedra form two different chains with $[Fe(1)_2O_6F_3]_\infty$ and $[Fe(2)_2O_6F_3]_\infty$ average composition, named chains **(1)** and **(2)**, respectively. Chains **(1)**, and **(2)** are extended along the [010] and [101] directions, respectively. In these chains there are two alternating Fe(1)–Fe(1) bond distances of 3.32(1) and 3.40(1) Å and two Fe(2)–Fe(2) bond lengths of 3.26(1) and 3.73(1) Å. The angle between these chains is approximately 120°.

An unusual feature in this crystal structure is the existence in each chain of two types of sequences, A and B, with a 50% of population, involving alternatively penta- and hexa-surrounding environments for the iron(II) cations (Fig. 4). This fact is caused by the disorder of the fluorine atoms. The refined crystal structure is the result of the superposition of these two sequences of iron(II) polyhedra in every chain. As a consequence of these facts, the connexion between the iron(II) polyhedra inside of each chain is through vertex- or edges-shared, alternatively. The two types of chains, **(1)** and **(2)**, are connected via a F-vertex common.

The arsenate tetrahedral groups are located between these two kinds of chains. The AsO_4 entities are tetradentate and linked to eight metallic cations through their four oxygen atoms. Every O(1) and O(2) is linked to two iron atoms, Fe(1) and Fe(2), whereas O(3) and O(4) are bonded to two Fe(2) and two Fe(1), respectively. In these arsenate groups, the mean value of the As–O bond distance is 1.68(1) Å, and the O–As–O angles range from 108.3(3)° to 111.7(3)°, as expected for the tetrahedral geometry with an sp^3 hybridization for the arsenic atoms.

2.5. Infrared, UV–vis and Mössbauer spectroscopies

The IR spectrum shows the bands corresponding to the vibrational modes of the $(AsO_4)^{3-}$ arsenate anion. The antisymmetric stretching vibration (ν_{as}) is detected as an intense split band at 895 and 820 cm^{-1}. The symmetric stretching mode (ν_s) is detected as a weak signal at 665 cm^{-1}. Finally, the antisymmetric deformation mode (δ_{as}) can be observed at 515 and 490 cm^{-1}. These vibrational modes are those usually found in arsenate compounds [16].

In the diffuse reflectance spectrum two bands at approximately 4000 and 9300 cm^{-1} are observed. These bands are characteristic of the iron(II) d^6 high spin cation in a distorted octahedral environment. The bands correspond to the electronic transitions from the $^5T_{2g}(^5D)$ fundamental state to the excited level $^5E_{2g}(^5D)$ which is split as consequence of the non-regular octahedral geometry observed for this cation. The energy associated to this transition corresponds, according to the Tanabe–Sugano diagram, to the D_q parameter [17], the value obtained being $D_q = 650\ cm^{-1}$. These results are in good agreement with those observed in other related compounds containing this metallic cation [18].

The Mössbauer spectrum, performed at room temperature in the paramagnetic state shows the presence of pure hyperfine interactions, and is formed by one doublet (Fig. 5). Taking into account the crystallographic data that indicate the existence of two crystallographically independent Fe(II) cations, the spectrum has been fitted to two doublets of Lorentzian using the NORMOS program [19]. As can be seen in Table 4, the isomer shift and quadrupole splitting values are in good agreement with

Table 4
Isomer shift (δ), quadrupolar splitting(ΔE) and relative spectral areas (% Fe) from the Mössbauer spectrum of $Fe_2(AsO_4)F$

Compound	Site	δ (mm s^{-1})	ΔE (mm s^{-1})	% Fe
$Fe_2(AsO_4)F$	Fe(1)	1.2150(1)	2.0435(1)	48(1)
	Fe(2)	1.2042(1)	2.6223(1)	52(1)

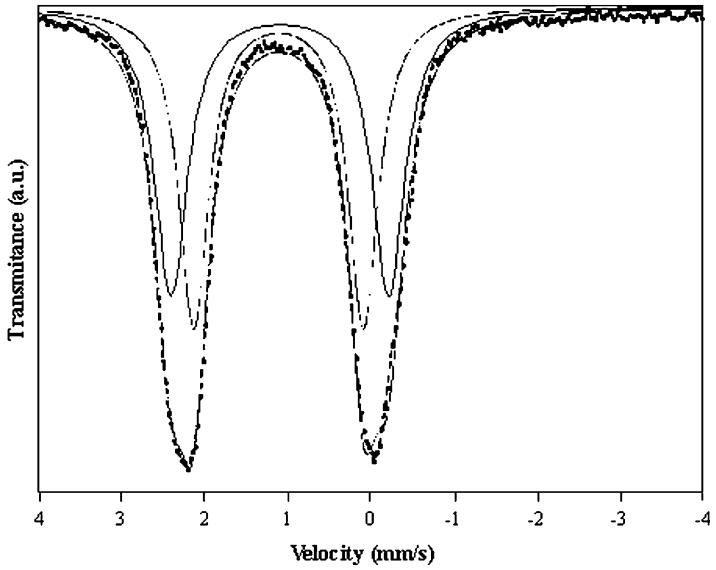

Fig. 5. Mössbauer spectrum of $Fe_2(AsO_4)F$ at 300 K.

those expected for the Fe(II) cations in octahedral geometry. The relative spectral areas are in the 1:1 ratio, in good accordance with the crystallographic multiplicities of the metallic cations.

2.6. Magnetic behavior

Magnetic measurements were performed on a powdered sample from room temperature to 5 K. Plots of the thermal evolution of χ_m and $\chi_m T$ are shown in Fig. 6.

The molar magnetic susceptibility increases with decreasing temperature and shows a maximum at approximately 22.6 K. This fact indicates the establishment of a long-range magnetic ordering, probably three dimensional in nature due the structural characteristic of this phase. The thermal evolution of χ_m follows the Curie–Weiss law at temperatures higher than 50 K. The calculated Curie and Curie–Weiss constants are $C_m = 7.67\,cm^3\,K/mol$ and $\theta = -76.4\,K$. The $\chi_m T$ vs. T curve decreases over the entire temperature range studied from $6.14\,cm^3\,K/mol$ at room temperature to $0.24\,cm^3K/mol$ at 5 K. Both the continuous decrease of the $\chi_m T$ product and the negative value of the Weiss temperature indicate the existence of antiferromagnetic interactions in this compound.

From the magnetic point of view, and taking into account the molecular field theory for a three-dimensional antiferromagnetic system [20], in which the susceptibility in the maximum is, approximately, 2/3 of the value of the susceptibility extrapolated to 0 K, the "J"-exchange parameter can be estimated from the following expression, $\chi_{max} = (N\beta^2 g^2/4zJ)$. For this equation, χ_{max} is the maximum value of the magnetic susceptibility, N is Avogadro's number, β is the Bohr magneton, and z is the

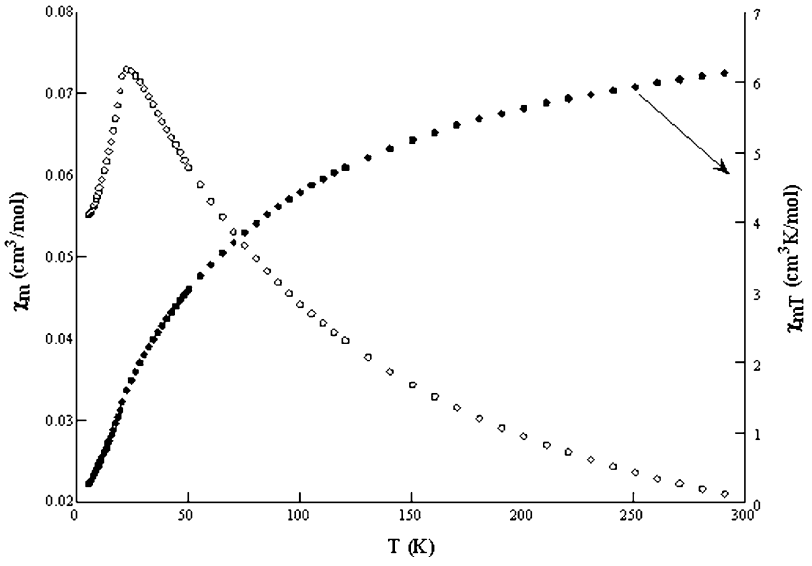

Fig. 6. Thermal evolution of χ_m and $\chi_m T$ of $Fe_2(AsO_4)F$.

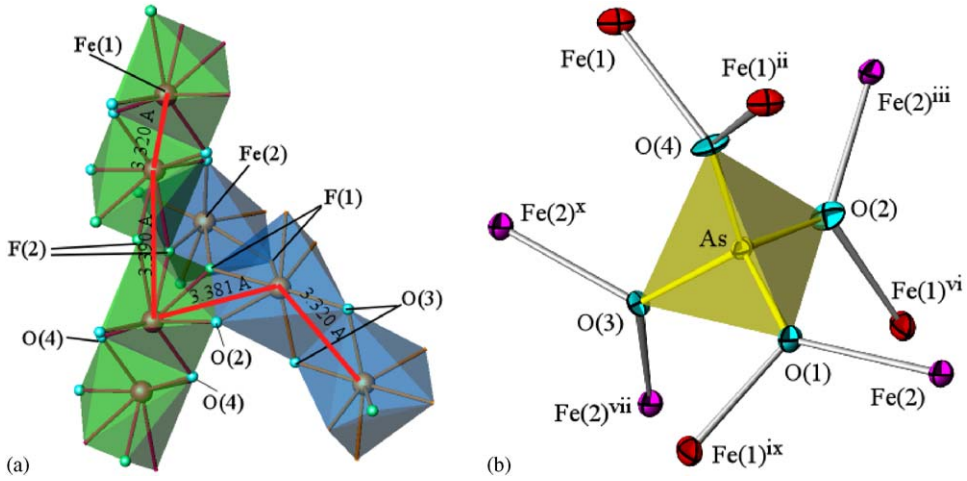

Fig. 7. Polyhedral view of the possible magnetic exchange pathways for $Fe_2(AsO_4)F$.

Table 5
Bond angles (°) for the possible magnetic exchange pathways in $Fe_2(AsO_4)F$

Angles	Values (°)
$Fe(1)^{ii}$–O(4)–Fe(1)	104.3(2)
Fe(1)–F(2)–$Fe(1)^{iv}$	133.6(5)
$Fe(2)^{xii}$–F(1)–$Fe(2)^{x}$	129.7(5)
$Fe(2)^{xi}$–O(3)–$Fe(2)^{x}$	102.2(2)
$Fe(1)^{ix}$–O(1)–Fe(2)	112.1(3)
$Fe(1)^{vii}$–O(2)–$Fe(2)^{iii}$	106.3(3)
Fe(1)–F(1)–$Fe(2)^{xii}$	130.6(6)
Fe(1)–F(1)–$Fe(2)^{x}$	99.7(4)
Fe(1)–F(2)–$Fe(2)^{xii}$	128.4(5)
$Fe(1)^{iv}$–F(2)–$Fe(2)^{xii}$	97.9(4)
Fe(2)–O(1)–As	130.6(2)
$Fe(1)^{ii}$–O(4)–As	128.6(1)
$Fe(2)^{iii}$–O(2)–As	129.9(1)
$Fe(2)^{x}$–O(3)–As	124.3(2)

Symmetry codes: i = x, $-y$, $z+1/2$; ii = $-x+1$, $-y$, $-z+1$; iii = $-x+1/2$, $y-1/2$, $-z+1/2$; iv = $-x+1$, $-y-1$, $-z+1$; v = $-x+1$, $-y-1$, $-z+1$; vi = $-x+1/2$,$-y+1/2$, $-z$; vii = $-x+1/2$, $y+1/2$, $-z+1/2$; viii = x, $-y$, $z-1/2$; ix = x, $-y$, $z+1/2$; x = x, $y-1$, z; xi = $-x+1$, y, $-z+1/2$; xii = $-x+1$, $y-1$, $-z+1/2$.

magnetic coordination number of a lattice site. Considering $g = 2.2(1)$ and $z = 5$ [20] the "J" value is -1.2 K.

Taking into account the average structural features of this phase, three magnetic exchange pathways can take place: (i) direct intermetallic interaction between the Fe(II) cations belonging to the $[Fe(1)O_4F_{1.5}]$ and $[Fe(2)O_4F_{1.5}]$ polyhedra, (ii) superexchange pathways between the iron(II) cations via oxygen and fluorine atoms (Fig. 7a) and (iii) super-superexchange interactions via arsenate anions (Fig. 7b). In the first pathway the intermetallic distances are greater than 3 Å, so, this pathway should be non-effective for the propagation of the magnetic interactions. However, in the second pathway, the deviation of the bond angles, shown in Table 5, from the orthogonal value of 90° should be effective in the propagation of antiferromagnetic interactions [21], as observed in the thermal evolution of the magnetic susceptibility. The latter pathway should favor the antiferromagnetic interactions, as observed in other related compounds [20].

3. Concluding remarks

A new fluorinated arsenate of iron(II) has been obtained by hydrothermal synthesis under autogenous pressure, using homopiperazine as a regulator of pH. The crystal structure contains chains with two kinds of sequences, A and B, with a 50% of population, involving alternatively penta- and hexa-surrounding environments for the iron(II) cations. The $(AsO_4)^{3-}$ anions are located in the holes delimited by the chains, with the oxygen anions linked to the metallic cation. From the diffuse reflectance spectrum, the D_q parameter has been calculated for the iron(II) cations in distorted octahedral environments. The Mössbauer spectrum performed at room temperature has allowed the values of the isomer shift and quadrupole splitting to be obtained, which are in good agreement with those habitually found for iron(II). The compound exhibits antiferromagnetic interactions with an estimated value for the "J"-exchange parameter of -1.2 K.

Acknowledgments

This work has been financially supported by the "Ministerio de Educación y Ciencia" (MAT2004-0271) and the "Universidad del País Vasco" (UPV/EHU) (9/UPV00130.310-13700/2001 and (9/UPV00169.310-13494/2001). The authors thank the technicians of SGIker, Dr. J.P. Chapman and Dr. I. Orue, financed by the National Program for the Promotion of Human Resources within the National Plan of Scientific Research, Development and Innovation, Ministerio de Ciencia y Tecnología and Fondo Social Europeo (FSE), for the X-ray diffraction and magnetic measurements, respectively. T. Berrocal wishes to thank the Gobierno Vasco/Eusko Jaurlaritza for funding.

Appendix A. Supplementary Materials

Supplementary data associated with this article can be found in the online version at doi:10.1016/j.jssc.2006.02.029.

References

[1] (a) S.M. Kauzlarich, P.K. Dorhout, J.M. Honig, J. Solid State Chem. 149 (2000) 3;
(b) C.N.R. Rao, J. Gopalakrihnan, New Directions in Solid State Chemistry. Structure, Synthesis, Properties, Reactivity and Materials Design, Cambridge University Press, 1986.
[2] R.C. Haushalter, Z. Wang, L.M. Meyer, S.S. Dhindra, M.E. Thomsonp, J. Zubieta, Chem. Mater. 10 (1998) 2801.
[3] (a) B. Bazan, J.L. Mesa, J.L. Pizarro, L. Lezama, J.S. Garitaonandia, M.I. Arriortua, T. Rojo, Solid State Sci. 5 (2003) 1291;
(b) S. Ekambaran, S.C. Sevov, Inorg. Chem. 39 (2000) 2405.
[4] Y.C. Liao, S.H. Luo, S.L. Wang, H.M. Kao, H.K. Lii, J. Solid State Chem. 155 (2000) 37.
[5] B. Bazan, J.L. Mesa, J.L. Pizarro, A. Goñi, L. Lezama, M.I. Arriortua, T. Rojo, Inorg. Chem. 40 (2001) 5691.
[6] (a) S.H. Luo, Y.C. Jiang, S.L. Wang, H.M. Kao, K.H. Lii, Inorg. Chem. 40 (2001) 5381;
(b) S. Chakrabarti, M.A. Green, S. Natarajan, Solid State Sci. 4 (2002) 405;
(c) S. Chakrabarti, S. Natarajan, Angew. Chem. Int. Ed. 41 (2002) 1224.
[7] (a) O. Najoua, M. Faouzi, J. Tahar, Acta Crystallogr. E (61) (2005) 167;
(b) F. Besma, B. Habib, J. Tahar, J. Solid State Chem. 173 (2) (2003) 273;
(c) A. Brahim, K. Mohamed, H. Amor, Acta Crystallogr. C (58) (2002) 198;
(d) H. Haas, M. Jansen, Z. Anorg. Allgemie Chem. 627 (5) (2001) 1013;
(e) J. Gaubicher, F. Orsini, T. Le Mercier, S. Llorente, A. Villesuzanne, J. Angenault, M. Quarton, J. Solid State Chem. 150 (2) (2000) 250;
(f) C. Masquelier, A.K. Padhi, K.S. Nanjundaswamy, J.B. Goodenough, J. Solid State Chem. 135 (2) (1998) 228.

[8] (a) H. Kessler, Stud. Surf. Sci. Catal. 52 (1989) 17;
(b) E. Torracca, U. Constantino, M.A. Massucci, J. Chromatogr. 30 (2) (1967) 584;
(c) G. Alberti, M. Casciola, U. Constantino, R. Vivan, Adv. Mater. 8 (4) (1996) 291.
[9] Powder Diffraction Files Inorganic and Organic, ICDD (a) 21–910, (b) 84–876, (c) 83–1554, (d) 83–1554. Pennsylvania, USA (1972).
[10] Oxford Diffraction Ltd. CRYSALIS Version 1.170.32 (2003).
[11] A. Altomare, G. Cascarano, C. Giacovazzo, A. Guagliardi, SIR92: A Program for Crystal Structure Solutión, 1993.
[12] G.M. Sheldrick, SHELXL97: Program for the Refinement of Crystal Structures, University of Göttingen, Germany, 1997.
[13] International Tables for X-ray Crystallography, vol VI, Kynoch Press, Birmingham, England, 1974, p. 99.
[14] E. Dowty, ATOMS: A Computer Program for Displaying Atomic Structures, Shape Software, 521 Hidden Valley Road, Kingsport, TN, 2000.
[15] (a) I.D. Brown, D. Altermatt, Acta Crystallogr. B 41 (1985) 244;
(b) N.E. Brsese, M. O'Keefee, Acta Crystallogr. B 47 (1991) 192.
[16] K. Nakamoto, Infrared and Raman Spectra of Inorganic and Coordination Compounds, Wiley, New York, 1997.
[17] A.B.P. Lever, Inorganic Electronic Spectroscopy, Elsevier Science Publisher BV, Amsterdarm, Netherlands, 1984.
[18] U.C. Chung, J.L. Mesa, J.L. Pizarro, L. Lezama, J.S. Garitaonandia, J.P. Chapman, M.I. Arriortua, J. Solid State Chem. 177 (2004) 2705.
[19] R.A. Brand, J. Larner, D.M. Herlach, J. Phys. F 14 (1984) 55.
[20] R.L. Carlin, Magnetochemistry, Springer, Berlin, Heidelberg, 1986.
[21] J.B. Goodenough, Magnetism and the Chemical Bond, Interscience, New York, 1963.

Further reading